ISSN 1063-7826, Semiconductors, 2019, Vol. 53, No. 5, pp. 662–666. © Pleiades Publishing, Ltd., 2019.
Russian Text © The Author(s), 2019, published in Fizika i Tekhnika Poluprovodnikov, 2019, Vol. 53, No. 5, pp. 669–673.

XVI INTERNATIONAL CONFERENCE "THERMOELECTRICS AND THEIR APPLICATIONS–2018" (ISCTA 2018), ST. PETERSBURG, OCTOBER 8–12, 2018

Miniaturized Heat-Flux Sensor Based on a Glass-Insulated Bi–Sn Microwire

L. A. Konopko[a,*], A. A. Nikolaeva[a], T. E. Huber[b], and A. K. Kobylianskaya[a]

[a] *Ghitu Institute of Electronic Engineering and Nanotechnology, Chisinau, MD-2028 Republic of Moldova*
[b] *Department of Chemistry, Howard University, Washington, DC 20059 USA*
**e-mail: l.konopko@nano.asm.md*

Received December 20, 2018; revised December 24, 2018; accepted December 28, 2018

Abstract—Thermoelectric-energy conversion based on a single element made of an anisotropic material is considered. In such materials, the heat flux generates a transverse electric field. We fabricate an experimental heat-flux sensor (HFS) sample consisting of a 10-m-long glass-insulated single-crystal tin-doped bismuth microwire (outer diameter $D = 18$ μm, microwire diameter $d = 4$ μm). The microwire is wound into a flat spiral after recrystallization in a strong electric field, during which the main crystallographic axis C_3 is oriented at the optimum angle with respect to the microwire axis. The sensor sensitivity reaches 10^{-2} V/W with the time constant $\tau \approx 0.2$ s. The sensor fabrication technology is rather simple and reliable for industrial applications.

DOI: 10.1134/S1063782619050117

1. INTRODUCTION

Currently, there is increased interest in the development of efficient thermoelectric materials for the fabrication of thermoelectric energy converters. At present, thermocouple elements based on the Seebeck and Peltier effects are most widely used. Such devices which possess undoubted advantages also have significant disadvantages, e.g., to obtain the necessary electrical voltages, they should be connected in series circuits; furthermore, technological problems arise in the development of low-resistance contacts to the *n*- and *p*-type legs of thermocouples; as a result, the reliability of device operation decreases.

One of the converters containing none of the aforementioned disadvantages is anisotropic thermoelements (ATs). In a crystal with anisotropic thermal conductivity, electrical conductivity, and a thermoelectric coefficient, if the heat-flux direction does not coincide with the main crystallographic axes, an electrical voltage is induced, which is perpendicular to the heat flux, proportional to the temperature difference between the isothermal sides, the thermoelectric-power anisotropy, crystal length, and inversely proportional to the crystal thickness [1–3]. ATs can be made of a single crystal of a suitable size and without any thermoelectric junction and, in contrast to thermocouples, have no problems with switching. One of the important applications of ATs is heat-flux measurement.

Heat-flux sensors (HFSs) are used in many cases, where it is important to gain an understanding of thermal-energy transfer processes. The Seebeck effect is used to measure the heat flux, where the signal is proportional to the temperature gradient, hence, the heat flux.

The signal of most HFSs based on this effect is proportional to their thickness; therefore, a high sensitivity at large thicknesses leads to a significant response time. In anisotropic HFS, the device can be sufficiently thin for a fast response to a variation in the heat flux (in an aerodynamic experiment, the HFS response time should be $\sim 10^{-6}$ s), while having a high signal level [4, 5].

The design of anisotropic thermoelectric devices requires materials with a high thermoelectric-power anisotropy. Recently discovered transverse ($p \times n$)-type thermoelements [6, 7], in which the thermoelectric power changes sign depending on mutually perpendicular crystallographic directions, have a high transverse thermoelectric power. The quasi-one-dimensional metal $Li_{0.9}Mo_6O_{17}$ has an extreme thermoelectric-power anisotropy along mutually perpendicular crystallographic axes (200 μV/K) [7]. ($p \times n$)-type materials allow the development of new variants of thermoelectric applications at the microscale and at cryogenic temperatures. A laser-induced transverse thermoelectric-power component was detected in inclined thin-film manganite oxide $La_{0.67}Ca_{0.33}MnO_3$ samples [8]. Strong thermoelectric-power anisotropy

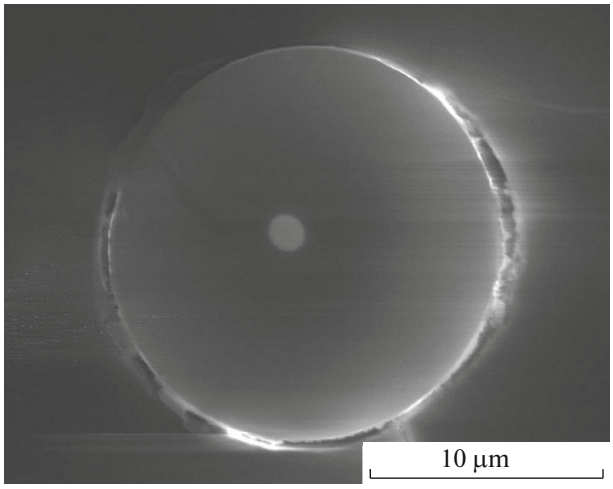

Fig. 1. SEM image of the cross section of a glass-insulated Bi-microwire; the outer and core diameters are D = 16.4 μm and d = 1.5 μm.

was observed in layered cobaltite Ca_xCoO_2 films [9], high-temperature superconductors $YBa_2Cu_3O_{7-\delta}$ [10] and $Bi_2Sr_2CaCu_2O_8$ [11] films. These samples can find potential application in fast and highly sensitive photodetectors. The effect was also observed using an artificial anisotropic medium consisting of an inclined multilayer structure [9, 12, 13].

This work is devoted to the continuation of the study (begun in [14, 15]) of the applicability of a single-crystal glass-insulated Bi and Bi–Sn microwire in designing and fabricating anisotropic thermoelectric devices such as anisotropic thermoelectric generators (ATG) and HTS.

2. EXPERIMENTAL

A single-crystal glass-insulated microwire made of pure and tin-doped bismuth was produced by the Ulitovsky method [16], i.e., high-frequency casting from the liquid phase into a glass capillary. Figure 1 shows a SEM image of the bismuth microwire cross section with the diameter (in terms of the glass insulation) D = 16.4 μm and core diameter d = 1.5 μm. The microwire is a cylindrical single crystal with the $(10\bar{1}1)$ orientation along the wire axis; in this orientation, the bisector axis C_1 is inclined to the wire axis in the bisector-trigonal plane at an angle of 19.5°; the trigonal axis C_3 is inclined from the wire axis by an angle of ~70°, and one of the binary axes C_2 is perpendicular to the wire axis. This method [17, 18] can be used to fabricate single-crystal wires with a core diameter d from 100 μm to 40 nm and up to several tens of meters long. To perform the studies, continuous Bi and Bi–Sn microwires with an inner core diameter d between 3 and 10 μm were fabricated.

The transverse thermoelectric power that arises at the microwire edges in the transverse temperature gradient is defined as $S_{trans} = U/\Delta T$, where U is the voltage across the sample and ΔT is the temperature gradient. To determine the optimum direction of the transverse temperature gradient in the microwire, a device was designed, consisting of two polished aluminum plates, 4.5 × 4.5 cm^2 in area at different temperatures T_2 and T_1. A microwire section ~10 cm long is between plates; in this case, a part of the section 4.5 cm long was in contact with the plates. In the case of a controlled shift of one of plates with respect to the other, the microwire was rotated in the transverse temperature gradient, which allowed recording of the dependence of the thermoelectric power on the temperature-gradient direction. To prevent microwire twisting during its rotation, contacts to the microwire edges were made using liquid InGa eutectic. A part of the wire section 1 cm long was placed between two neodymium magnets inducing a transverse magnetic field of ~0.5 T, which make it possible to measure the rotation diagram of the transverse magnetoresistance of the microwire; thus to determine the orientation of the crystallographic axes of the microwire [15]. Use of the microwire in anisotropic thermoelectric converters, e.g., by winding it into a flat spiral, imposes certain requirements on the orientation of the main crystallographic axes of the microwire [14, 15]. To provide the maximum AT output voltage, a setup for recrystallizing the microwire in a strong electric field was produced. All measurements of the transverse microwire thermoelectric power were performed at room temperature.

3. RESULTS AND DISCUSSION

Figure 2 schematically shows a rectangular single-crystal bismuth sample whose two opposite faces are at different temperatures; due to the anisotropy of the thermoelectric power, the thermal conductivity, and the electrical conductivity along the sample, a voltage E perpendicular to the temperature gradient $\Delta T = T_2 - T_1$ arises, which is proportional to the sample length, thermoelectric-power anisotropy, and inversely proportional to its thickness [1, 2, 19],

$$E = \alpha_{12}\Delta T\frac{a}{b} = (\alpha_{33} - \alpha_{11})\sin\beta\cos\beta\Delta T\frac{a}{b}$$
$$= (\alpha_{33} - \alpha_{11})\sin\beta\cos\beta\frac{Q_z}{w(\kappa_{33}\sin^2\beta + \kappa_{11}\cos^2\beta)}, \quad (1)$$

where α_{11}, α_{33} is the thermoelectric power along the C_1 and C_3 axes, respectively, $(\alpha_{11} - \alpha_{33})$ is the thermoelectric-power anisotropy, β is the inclination angle of the crystallographic C_3 axis with respect to the sample axis, ΔT is the transverse temperature gradient, a is the sample length, b is the sample thickness, w is the sample width; κ_{11} and κ_{33} are the thermal conductivity along C_1 and C_3 axes, respectively; Q_z is the heat flux

through the sample, $Q_z = q_z aw$, and q_z is the heat flux through the unit area, $q_z = (T_2 - T_1)/b\,(\kappa_{33}\sin^2\beta + \kappa_{11}\cos^2\beta)$.

In the glass-insulated bismuth microwire samples ($D = 20$ μm, $d = 6.9$ μm), the transverse thermoelectric-power maximum is reached when the C_3 axis in the microwire is directed along the temperature gradient, $S_{trans} = 350$ μV/K (for a microwire section 4.5 cm long, in contact with two plates at different temperatures T_2 and T_1). The bismuth thermoelectric-power anisotropy at room temperature is $\alpha_{33} - \alpha_{11} = 40$ μV/K. To achieve higher transverse thermoelectric powers, we used tin-doped bismuth, i.e., Bi–0.05 at % Sn, in which the thermoelectric-power anisotropy is $\alpha_{33} - \alpha_{11} = 60$ μV/K [15]. In glass-insulated Bi–0.05 at % Sn microwire samples ($D = 18$ μm, $d = 4$ μm), $S_{trans} = 629$ μV/K.

The AT volt–watt sensitivity is given by

$$s = \frac{E}{Q_z} = \frac{(\alpha_{33} - \alpha_{11})\sin\beta\cos\beta}{w(\kappa_{33}\sin^2\beta + \kappa_{11}\cos^2\beta)}. \quad (2)$$

For the Bi samples, the maximum sensitivity is achieved at the angle

$$\beta_{opt} = \pm\arctan\sqrt{\frac{\kappa_{11}}{\kappa_{33}}} = 52.78^\circ. \quad (3)$$

To achieve efficiency of the anisotropic device based on Bi, the axis C_3 inclination angle with respect to the microwire axis should be $\beta = 52.8^\circ$. We developed a new recrystallization technology of glass-insulated single-crystal Bi and Bi–Sn microwires in a strong electric field. This technology makes it possible to change the main C_3 crystallographic axis in the microwire with respect to the electric-field direction. After recrystallization of the glass-insulated microwire, it can be bent to a radius of 2 mm without destruction. This feature allowed AT fabrication [20] using the developed recrystallization technology for microwire winding into a flat spiral immediately at the setup output; therewith, the C_3 axis orientation in the microwire (top panel of Fig. 2) was identical at all spiral points, which provided the maximum possible thermoelectric figure of merit of the device. After recrystallization in a strong electric field, the transverse thermoelectric power in glass-insulated Bi–0.05 at % Sn microwire samples ($D = 18$ μm, $d = 4$ μm) reached $S_{trans} = 730$ μV/K. To obtain an AT output voltage of 1 V at a transverse temperature gradient $\Delta T = 5$ K, 12 m of this microwire should be used for winding into a spiral. The AT resistance will be $R = 1$ MΩ, and the maximum current of this generator will be ~1 μA. We fabricated an experimental ATG sample using 10 m of Bi–0.05 at % Sn microwire ($D = 20$ μm, $d = 4$ μm), wound into a flat spiral.

In the last stage of ATG fabrication, a copper radiator was glued to the flat spiral. The experimental ATG sample placed in contact with the surface at a temperature of 36°C (temperature of a human hand) showed a peak voltage of 210 mV; however, the voltage under steady-state conditions decreased to 10 mV.

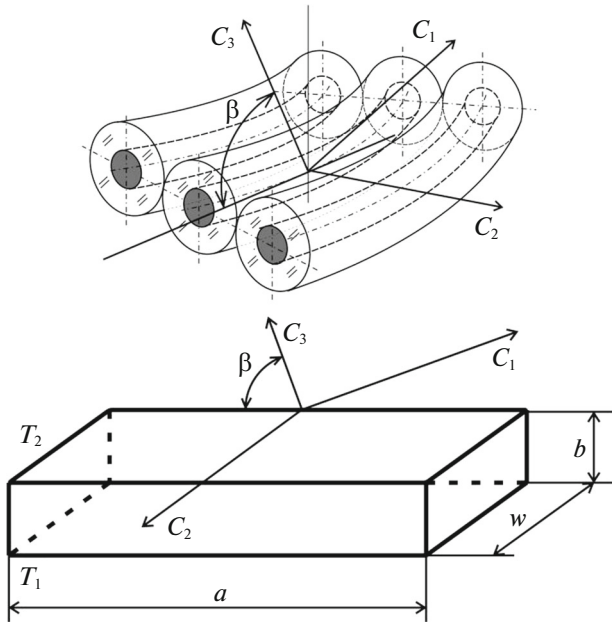

Fig. 2. Anisotropic thermoelement made of (bottom) bulk single crystal and (top) by winding a glass-insulated single-crystal microwire into a flat spiral; C_1, C_2, C_3 are the main crystallographic axes.

The AT thermoelectric figure of merit Z_a depends on the thermoelectric-power anisotropy $\Delta\alpha = \alpha_{33} - \alpha_{11}$ [1, 2, 6],

$$Z_a = \frac{(\alpha_{33} - \alpha_{11})^2 \sin^2\beta\cos^2\beta}{(\kappa_{33}\sin^2\beta + \kappa_{11}\cos^2\beta)(\rho_{33}\cos^2\beta + \rho_{11}\sin^2\beta)}, \quad (4)$$

where κ_{11} and κ_{33} are the thermal-conductivity tensor components and ρ_{11} and ρ_{12} are the resistivity tensor components. In the samples under study, the microwire-core diameter is rather large; therefore, the room-temperature size effect in the resistivity and thermal conductivity can be neglected. To estimate the thermoelectric figure of merit Z_a of the device under study, the following resistivity and thermal conductivity bulk bismuth samples [21] were used: $\rho_{33} = 1.34 \times 10^{-6}$ Ω m, $\kappa_{33} = 6$ W/(m K), $\rho_{11} = 1.11 \times 10^{-6}$ Ω m, $\kappa_{11} = 9.9$ W/(m K). Then for $\beta = 52.8^\circ$, $\alpha_{33} - \alpha_{11} = 6 \times 10^{-4}$ V/k, we obtain $Z_a = 0.94 \times 10^{-4}$ K^{-1} and $Z_aT = 2.8 \times 10^{-2}$ at $T = 300$ K. We can see that the thermoelectric figure of merit is low for using the anisotropic thermoelement as an energy generator; however, ATs are widely used as sensors [1].

A Bi–0.05 at % Sn microwire ($D = 20$ μm, $d = 4$ μm) 9.9 m long, wound into a flat spiral, was used to fabricate an experimental HFS sample. At a high sensitivity (s ~ 10 mV/W), the HFS exhibited a fast response time. A block diagram of the setup for studying the response time in the developed HFS is shown in

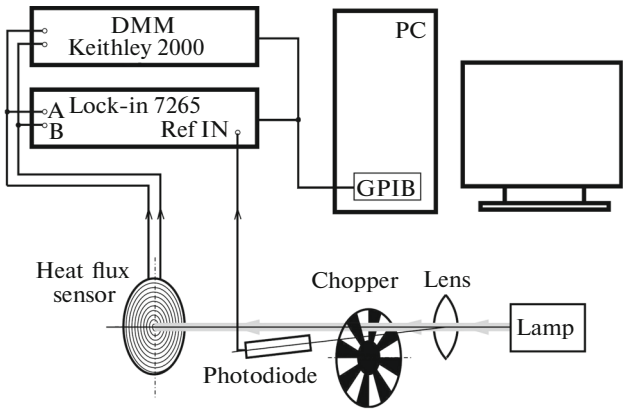

Fig. 3. Block diagram of the setup for determining the HFS response time. The illuminator of the MBS-9 microscope was used.

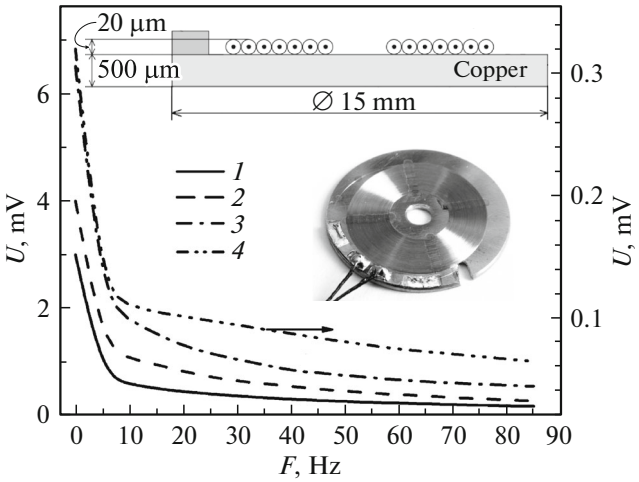

Fig. 4. Dependence of the HFS output voltage on the light-flux modulation frequency. The HFSs were fabricated of glass-insulated Bi–0.05 at % Sn microwire with various lengths and diameters: (*1*) $L = 7.7$ m, $d = 5$ μm, $R = 352$ kΩ; (*2*) $L = 9.9$ m, $d = 4$ μm, $R = 1040$ kΩ; (*3*) $L = 6$ m, $d = 4$ μm. $R = 675$ kΩ; (*4*) $L = 0.3$ m, $d = 4$ μm, $R = 35$ kΩ. The insets show: (top) HFS block diagram and (center) HFS external view.

Fig. 3. As a radiation source, the illuminator of an MBS-9 stereomicroscope was used. Light from the source, having passed through a modulator, was incident on the HFS and on an additional photodiode generating the modulation frequency necessary for synchronous detection. The FHS signal was recorded by a Lock-in Amplifier 7265 synchronous detector and, under steady-state conditions, by a Keithley 2000 digital multimeter. Bi–0.05 at % Sn microwires of various lengths L were used to fabricate four FHS samples: $L = 9.9$ m, $d = 4$ μm, $R = 1040$ kΩ; $L = 7.7$ m, $d = 5$ μm, $R = 352$ kΩ; $L = 6$ m, $d = 4$ μm, $R = 675$ kΩ; $L = 0.3$ m, $d = 4$ μm, $R = 35$ kΩ. Figure 4 shows the dependence of the HFS voltage U on the light-modulation frequency (F). The response time for all samples is $\tau \approx 0.22$ s and is independent of the sensor resistance at low frequencies. Such a slow sensor response in comparison with the bulk HFS samples based on Bi, where $\tau \approx 5 \times 10^{-5}$ s [5], can be explained by the presence of thick (7 μm) glass insulation of the microwire. The fabricated experimental samples (HFS schematic diagram and external view are shown in the insets of Fig. 4) show that a single-crystal Bi–0.05 at % Sn microwire wound into a flat spiral can be used in anisotropic thermoelectric devices. In this case, the fabrication technology is rather simple and reliable for industrial applications.

4. CONCLUSIONS

The fabrication technology of sensitive HFSs made of glass insulated single-crystal Bi–0.05 at % Sn microwire was developed. A microwire segment 9.9 m long ($D = 18$ μm, $d = 4$ μm) was wound into a flat spiral after recrystallization in a strong electric field, during which the main crystallographic axis C_3 was oriented at the optimum angle to the microwire axis to achieve a maximum efficiency. The HFS sensitivity reached 10^{-2} V/W. Various HFS samples made of microwire segments with different lengths $L = 0.5$–9.9 m, having a resistance spread of $R = 35$–1040 kΩ showed an approximately identical response time, $\tau \approx 0.22$ s. The presence of the thick glass coating of the microwire, 7 μm, is most likely the cause of a significant increase in the response time in comparison with bulk Bi HFS samples. The fabrication technology of the developed HFSs is rather simple and reliable for industrial applications.

FUNDING

This study was supported by the IEEN Institutional project no. 15.817.02.09A, the National Science Foundation (grant no. STC CIQM 1231319), the Boeing company, and Keck Foundation.

REFERENCES

1. A. A. Snarskii, A. M. Pal'ti, and A. A. Ashcheulov, Semiconductors **31**, 1101 (1997).
2. A. A. Snarskii and L. P. Bulat, in *Thermoelectrics Handbook: Macro to Nano*, Ed. by D. M. Rowe (CRC, New York, 2006), Chap. 45.
3. L. I. Anatychuk and A. V. Prybyla, J. Electron. Mater. **40**, 1304 (2011).
4. S. Z. Sapozhnikov, V. Yu. Mitiakov, and A. V. Mitiakov, Tech. Phys. **49**, 920 (2004).
5. S. V. Bobashev, N. P. Mende, P. A. Popov, B. I. Reznikov, V. A. Sakharov, S. Z. Sapozhnikov, V. Yu. Mityakov, A. V. Mityakov, D. A. Buntin, A. A. Maslov, H. Knauss, and T. Roediger, Tech. Phys. Lett. **35**, 214 (2009).

6. Y. Tang, B. Cui, C. Zhou, and M. Grayson, J. Electron. Mater. **44**, 2095 (2015).
7. J. L. Cohn, S. Moshfeghyeganeh, C. A. M. dos Santos, and J. J. Neumeier, Phys. Rev. Lett. **112**, 186602 (2014).
8. K. Zhao, K.-J. Jin, Y.-H. Huang, H.-B. Lu, M. He, Z.-H. Chen, Y.-L. Zhou, and G.-Z. Yang, Phys. B (Amsterdam, Neth.) **373**, 72 (2006).
9. T. Kanno, K. Takahashi, A. Sakai, H. Tamaki, H. Kusada, and Y. Yamada, J. Electron. Mater. **43**, 2072 (2014).
10. Z. H. He, Z. G. Ma, Q. Y. Li, Y. Y. Luo, J. X. Zhang, R. L. Meng, and C. W. Chu, Appl. Phys. Lett. **69**, 3587 (1996).
11. Th. Zahner, R. Schreiner, R. Stierstorfer, O. Kus, S. T. Li, R. Roessler, J. D. Pedarunig, D. Baüerle, and H. Lengfellner, Europhys. Lett. **40**, 673 (1997).
12. K. Fischer, C. Stoiber, A. Kyarad, and H. Lengfellner, Appl. Phys. A **78**, 323 (2004).
13. S. A. Ali and S. Mazumder, Int. J. Heat Mass Transf. **62**, 373 (2013).
14. L. Konopko, A. Nikolaeva, T. Huber, and A. Tsurkan, IFMBE Proc. **55**, 119 (2016).
15. L. A. Konopko, A. A. Nikolaeva, A. K. Kobylianskaya, and T. E. Huber, J. Electron. Mater. **47**, 3171 (2018).
16. V. S. Larin, A. V. Torcunov, A. Zhukov, J. González, M. Vazquez, and L. Panina, J. Magn. Magn. Mater. **249**, 39 (2002).
17. N. B. Brandt, D. V. Gitsu, A. A. Nikolaeva, and Ya. G. Ponomarev, Sov. Phys. JETP **45**, 1226 (1977).
18. D. Gitsu, L. Konopko, A. Nikolaeva, and T. Huber, Appl. Phys. Lett. **86**, 102105 (2005).
19. A. Mityakova, S. Sapozhnikov, V. Mityakov, A. Snarskii, M. Zhenirovsky, and J. Pyrhonena, Sens. Actuators A **176**, 1 (2012).
20. L. Konopko, A. Nikolaeva, P. Bodiul, and A. Tsurkan, MD Patent No. 4333 (2015).
21. C. F. Gallo, B. S. Chandrasekhar, and P. H. Sutter, J. Appl. Phys. **34**, 144 (1963).

Translated by A. Kazantsev